

Room-Temperature Broad-Wavelength-Tunable Single-Mode Lasing from Alloyed $\text{CdS}_{1-x}\text{Se}_x$ Nanotriopods

Pengfei Guo,^{*,#} Qian Yang,[#] Xia Shen,[#] Qihang Lv, Yuying Hao, Liantuan Xiao,^{*} Johnny C. Ho,^{*} and Kin Man Yu^{*}



Cite This: *ACS Nano* 2022, 16, 12767–12776



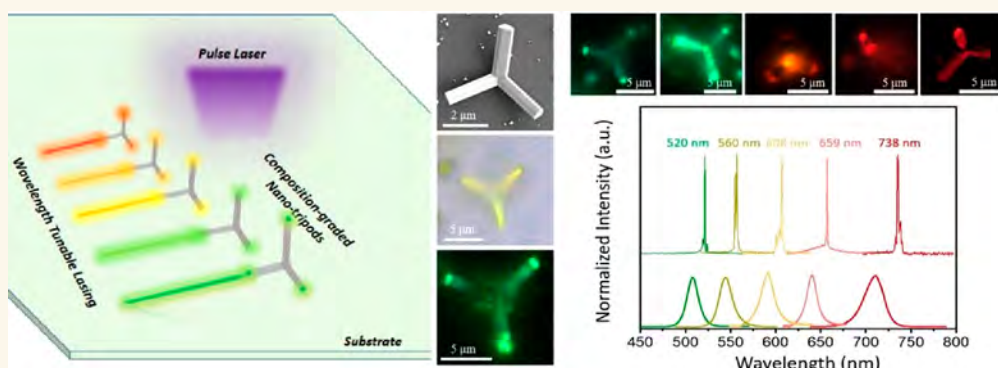
Read Online

ACCESS |

Metrics & More

Article Recommendations

Supporting Information



ABSTRACT: Wavelength-tunable semiconductor nanolasers have attracted tremendous attention for their tunable emissions and robust stability, bringing possibilities for various applications, including nanophotonic circuits, solid-state white-light sources, wavelength-converted devices, and on-chip optical communications. Here, we report on the demonstration of broadband-tunable, single-mode nanolasers based on high-quality alloyed single crystalline $\text{CdS}_{1-x}\text{Se}_x$ ($x = 0\text{--}1$) nanotriopods with well-formed facets fabricated using a conventional CVD approach. Microstructural characterization and optical investigations reveal that these structures are crystalline with composition-tunable $\text{CdS}_{1-x}\text{Se}_x$ alloys. Microphotoluminescence spectra and mapping of these nanotriopods exhibit emissions with continuous wavelengths from 509 to 712 nm, further demonstrating that the $\text{CdS}_{1-x}\text{Se}_x$ alloys have tunable bandgaps due to the composition gradient. Additionally, under a pulse laser illumination, room-temperature single-mode lasing is clearly observed from these nanotriopods cavities, which shows almost identical emission lines with a high-quality factor of ~ 1231 . More importantly, wavelength continuously tunable nanolasers from 520 to 738 nm are successfully constructed using these bandgap gradient nanotriopods. The capability to fabricate high-quality tunable nanolasers represents a significant step toward high-integration optical circuits and photonics communications.

KEYWORDS: semiconductor, nanotriopods, bandgap modulation, wavelength-tunable nanolasers, nanophotonics

INTRODUCTION

The ability to engineer and control bandgaps of semiconductors through alloying is one of the essential attributes that makes semiconductors useful for many optoelectronic applications.^{1–5} Semiconductor nanostructures offer an opportunity in tunable optoelectronic devices for their greater flexibility in composition control and bandgap modulation.^{6,7} Recently, wavelength-tunable lasers of bandgap modulated semiconductor nanostructures have attracted considerable interest because of their potential applications in future photonic and optoelectronic devices,^{1,2,8–10} for instance, solid-state lighting, lasers, optical

data storage and optical communication.¹¹ However, it is still challenging for nanoscale lasers to achieve room-temperature

Received: May 11, 2022

Accepted: July 28, 2022

Published: August 2, 2022



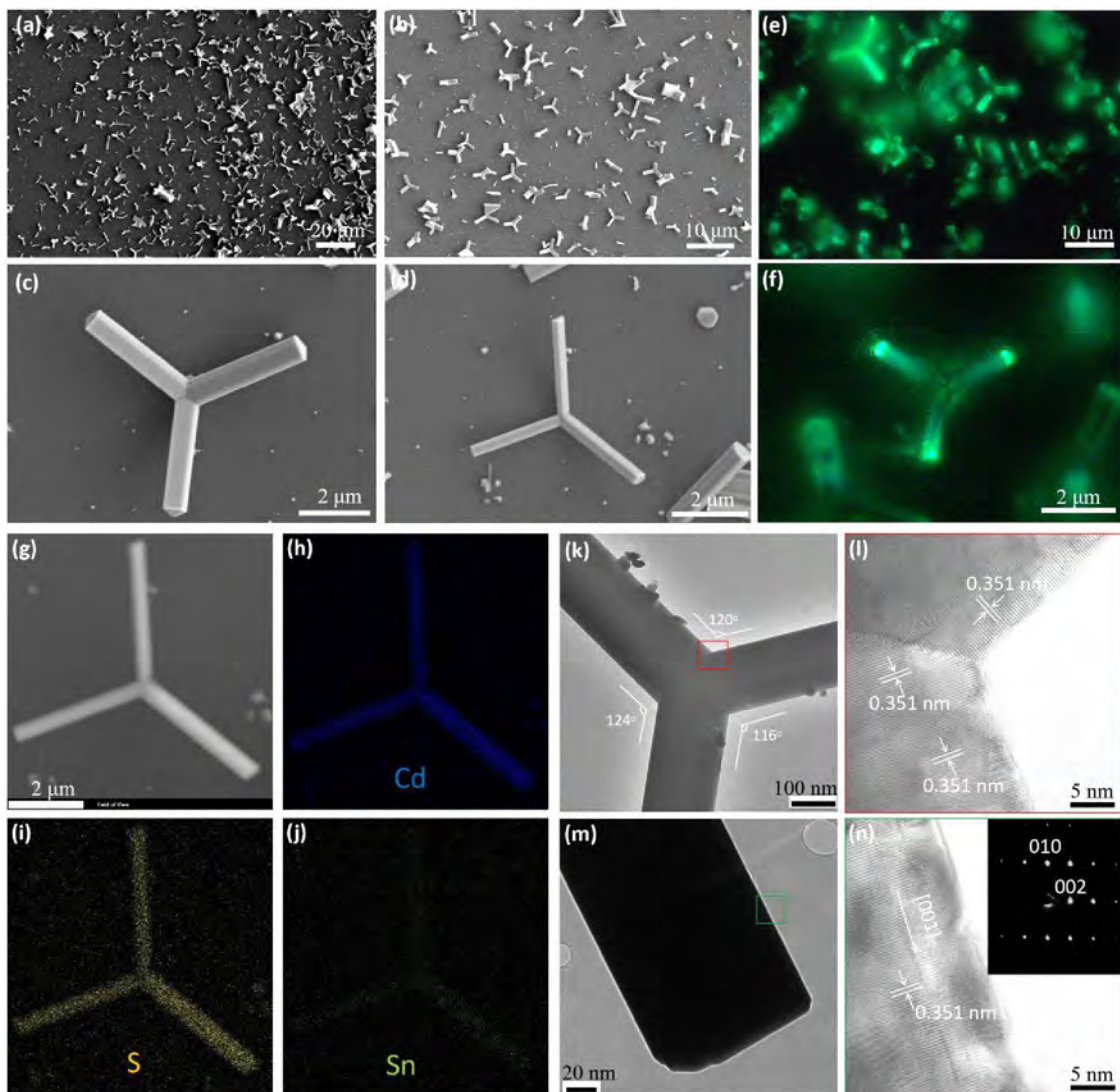


Figure 1. Structural characterization of Sn-doped CdS nanotripods. (a and b) Low-resolution top-view SEM images of CdS nanotripods grown on the silicon substrate. (c and d) Close-up SEM images of two typical CdS nanotripods with three legs at projection angles of about 120°. (e) A dark-field real-color photograph of some selected nanotripods and (f) a typical single structure under an unfocused 355 nm pulsed laser illumination. (g–j) SEM images and EDS maps for Cd, S, and Sn elements of a typical nanotriod. (k) A low-resolution TEM image of a CdS nanotriod. (l) HRTEM image focused on the interface of two branches. (m) A low-resolution TEM image of the right branch from the CdS nanotriod. (n) A HRTEM image from one branch of the nanotriod. Inset: the corresponding SAED pattern from the nanotriod.

lasing emission with an extremely broad wavelength range.^{4,12–14}

Additionally, semiconductor nanostructures offer superior end face¹⁵ and stronger optical confinement compared to results for components constructed by the top-down method.¹⁶ They are therefore ideal candidates for optical gain materials and nanoscale optical cavities for understanding nanoscale lasers.^{17–20} To date, various nanolasers have been demonstrated on the basis of many self-assembled single-crystalline semiconductor nanostructures, including nanocrystals,^{21–23} nanowires,^{4,9,24,25} nanoribbons,^{26,27} heterostructures,^{28,29} nanoplatelets,^{30–32} and nanobeam.³³ Especially, most tunable nanoscale lasers are constructed and realized on the basis of the conventional Fabry-Pérot (F-P) cavities or whispering-gallery-mode (WGM) cavities by changing the composition of the semiconductor structures.^{8,34–42} Tunable lasers can fulfill a number of roles relevant to nanophotonic applications.^{34–36} For example, bandgap-tunable CdS_{1-x}Se_x nanobelts with their band

gap ranging from 2.42 to 1.74 eV were realized, which shows a tunable F-P lasing emission from 710 to 510 nm under a pulsed laser excitation.^{11,37} Similarly, Zn_yCd_{1-y}S alloy nanoribbons exhibit F-P lasing emission from 510 to 340 nm under optical pumping.^{38,39} All-inorganic cesium lead halide CsPbX₃ (X = Cl, Br, I) crystalline microcavities were reported for tunable WGM lasing over the entire visible region (410–700 nm).³⁴ Composition-tunable single-mode plasmonic lasing from 474 to 627 nm were realized by In_xGa_{1-x}N@GaN core-shell nanorods supported on an Al₂O₃-capped epitaxial Ag film.⁴² Yang et al. used single on-wire bandgap-graded CdS_{1-x}Se_x nanowires and realized broadly tunable F-P nanolasers over a wide visible range up to 119 nm by forward cutting the alloy nanowire from the CdSe to the CdS end.⁸ Besides these examples of tunable lasers based on structures with gradient compositions, waveguide embedded plasmon lasers multiplexed onto a single CdS nanobelt with 490–502 nm, allowing efficient electrical modulation, were also reported. These findings further

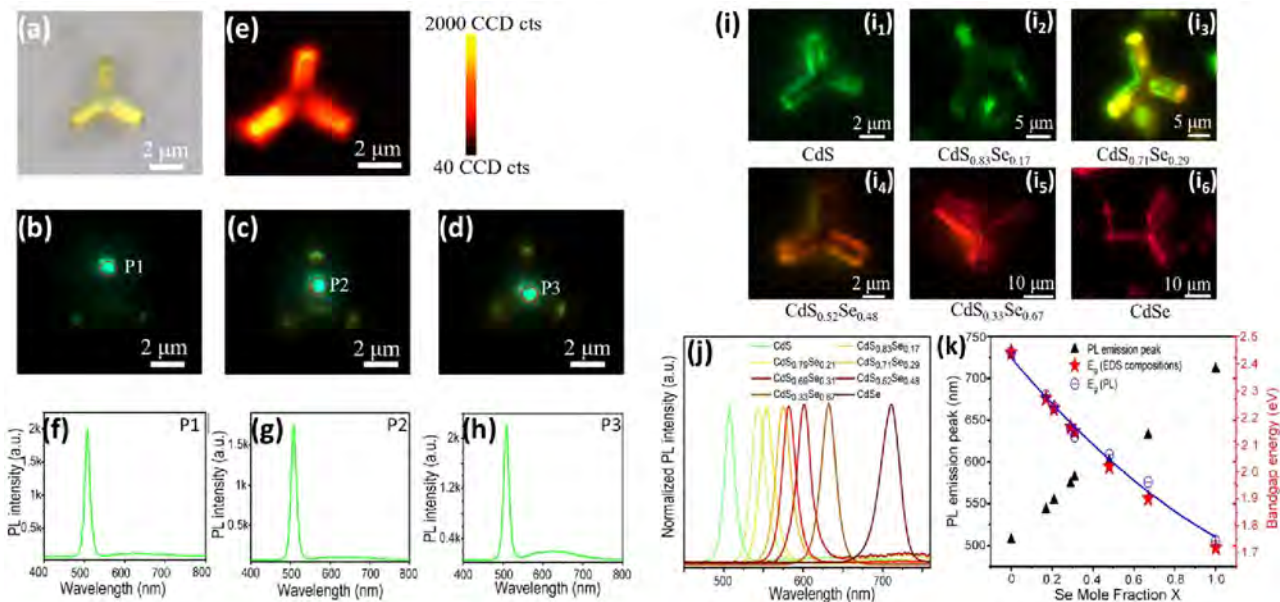


Figure 2. Optical characterization of CdS_{1-x}Se_x nanotripods. (a) An optical photograph of a typical Sn-doped CdS nanotri pod. (b-d) Dark-field emission images excited by a focused 488 nm laser at three typical positions (P₁–P₃), respectively. (e) 2D emission mapping of this Sn-doped CdS nanotri pod. (f-h) Corresponding PL spectra from three positions P₁–P₃, indicated in (b-d). (i) Real-color images of CdS_{1-x}Se_x alloy nanotripods with various compositions and (j) corresponding PL spectra of CdS_{1-x}Se_x alloy nanotripods showing the continuous variation of the emission peak because of different compositions. (k) Plots correlating the emission wavelengths and bandgaps of CdS_{1-x}Se_x nanotripods as a function of alloy composition. The solid line shows the best fit of composition-dependent bandgaps using the virtual crystal approximation with a bowing parameter $b = 0.23$ eV.

demonstrated the potential of multicolor plasmon lasers for photonic integration.⁴⁰ Wavelength-tunable F-P nanolasers of CdSe and CdS nanowires with the emitted wavelengths ranging from 706 to 746 nm and 489 to 520 nm, respectively, were reported on the basis of the absorption–emission–absorption process.^{41,43} Despite all this extraordinary progress, tunable nanoscale lasers and multicolor emissions of artificial multi-functional resonators are urgently needed for further applications in ultrafast information processing.

Although wide-wavelength-tunable lasers have been realized by F-P cavities or WGM cavities using different semiconductor nanowires/ribbons or nanoplatelets as gain media,^{10,25,34,44,45} such laser structures based on single-nanotri pod cavities, to the best of our knowledge, never have been reported. In this paper, we demonstrate an efficient way to achieve wide-wavelength-tunable lasers on single-composition-tunable CdS_{1-x}Se_x ($x = 0$ –1) nanotripods, which were synthesized by a bottom-up self-assembly CVD approach. Structural characterization reveals that these nanotripods have high crystalline quality with a wurtzite structure and exhibit a fine tridimensional nanotri pod structure with the vertical projection angle of the three arms about 120°. Spatially resolved microphotoluminescence (μ -PL) spectra and optical scanning PL mapping images indicate a series of narrow emission bands from 509 to 712 nm, changing by the bandgap modulation. Optically pumped lasing with a single mode is observed using a nanotri pod F-P cavity, and the lasing modes show a red shift depending on the increasing size of the tri pod resonant cavity. Moreover, wavelength-tunable nanolasers can be achieved continuously from 520 to 738 nm by varying the composition of the CdS_{1-x}Se_x nanotripods. These nanotri pod-based tunable lasers have potential applications in constructing compact nanophotonic components.

RESULTS AND DISCUSSION

Low- and high-resolution scanning electron microscopy (SEM) images (Figure 1a–d) show that the as-grown structures are nanotripods with three crystal legs of 2–18 μ m in length and 100–500 nm in diameter. As can be seen from Figure 1c,d, the nanotri pod structures grow directly on a silicon substrate, and the part near the center of the tri pod is directly connected with the substrate without any intermediate structure or buffer layer, while the three legs grow obliquely upward from the center (Figure S1, Supporting Information). A dark-field real-color image of the nanotri pod structures and a typical real-color emission image of a single nanotri pod under a 355 nm laser illumination shown in Figure 1e,f, respectively, suggest that the nanotripods have uniform emissions with the green light from three legs. The clearly observed bright spots at the tip of nanotripods indicate good waveguide effects of the light in these tri pods structures (Figure 1f).

Figure 1 panels g–j show the SEM images and 2D elemental mapping of a typical nanotri pod. The EDS spectrum shows that Cd, S, and Sn are present in the nanotri pod (Figure S2, Supporting Information), and the atomic ratio of S and Cd is close to 1:1 with $\sim 1.92\%$ Sn. Two-dimensional (2D) elemental mappings for the three detected elements (Cd, S, and Sn) are shown in Figure 1h–j, suggesting a uniform distribution of the three elements along the nanotripods. One representative nanotri pod was picked up and placed on a microgrid by a homemade fiber taper under an optical microscope for structural characterization, as shown in Figure S3 (Supporting Information). The microstructure of this nanotri pod was investigated by transmission electron microscopy (TEM). Figure 1k is a typical low-resolution TEM image of the selected nanotri pod showing three legs with straight and smooth edges connecting with each other at projection angles of 120°, 116°, and 124°, respectively.

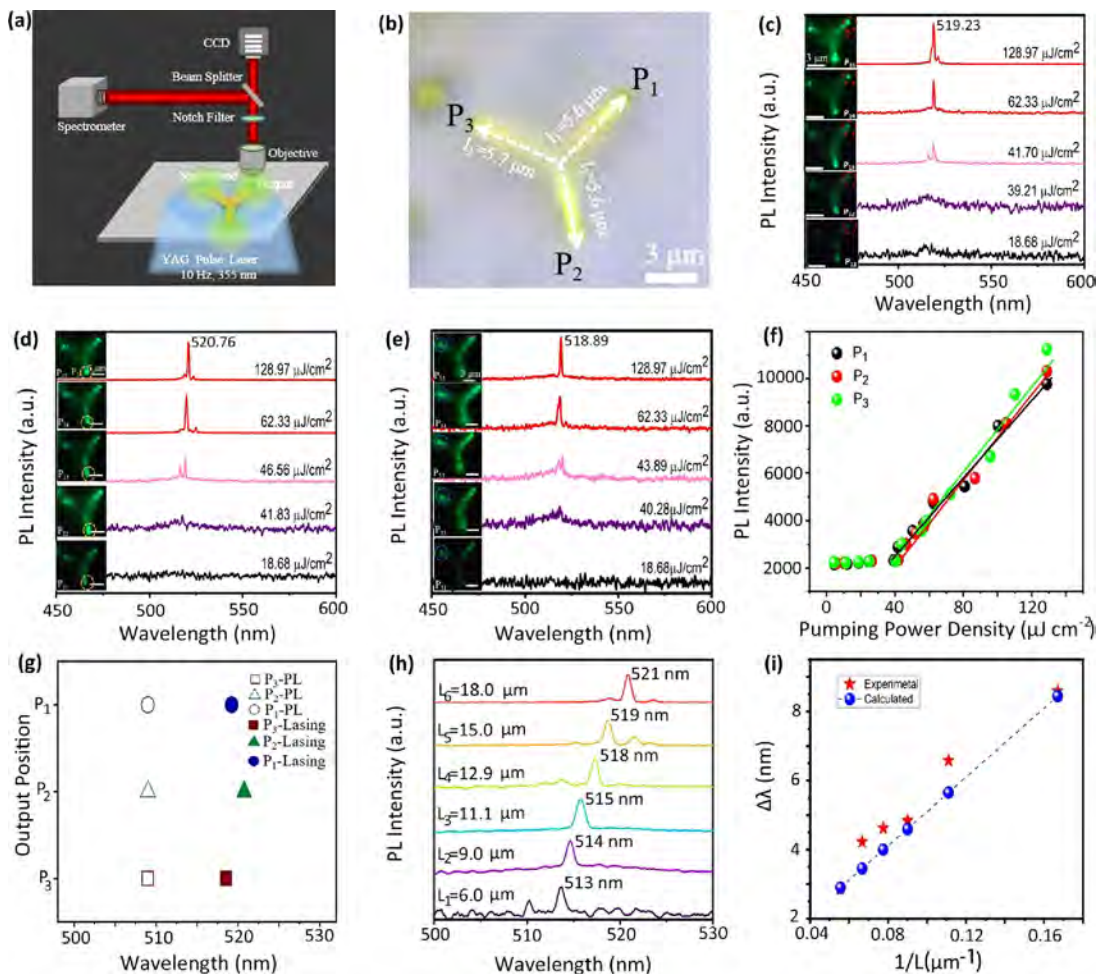


Figure 3. Room-temperature lasing emissions of Sn-doped CdS nanotriplets. (a) A schematic diagram of the experimental setup for the lasing measurements on an Sn-doped CdS nanotriplet. The structure is under the illumination of an unfocused 355 nm pulse laser beam. (b) A top-view optical photograph of the CdS nanotriplet showing the lengths of the three legs. (c–e) Pumping power-dependent room-temperature PL spectra from three legs (P₁–P₃) of a CdS nanotriplet as indicated in (b), respectively. Insets show the corresponding dark-field real-color images. The scale bars in the insets are 3 μm. (f) Pumping power-dependent emission intensity from the three spots (P₁–P₃) at ~520 nm. (g) PL emission and lasing wavelengths from the three spots of the nanotriplet. (h) Size-dependent lasing emission wavelength of some nanotriplets from 6.0 to 18.0 μm. (i) The mode spacing, $\Delta\lambda$ plotted as a function of 1/L (L is the equivalent cavity length) for the corresponding cavities in (h). Red star symbols are the experimental data, and blue sphere symbols are the calculated data according to eq 2.

The corresponding high-resolution TEM (HRTEM) image at the junction (red square in Figure 1k) is exhibited in Figure 1l, which shows a high-quality single-crystalline microstructure with the lattice spacing of ~0.351 nm, corresponding to the (002) lattice spacing of wurtzite CdS. Figure 1 panels m and n show the low- and high-resolution TEM images at the tip of the nanotriplet, respectively. Similar to Figure 1l, the (002) lattice spacing of wurtzite CdS of ~0.351 nm is also measured. The corresponding selected area electron diffraction (SAED) pattern (inset in Figure 1n) shows well-arrayed diffraction spots, indicating a high-quality single-crystalline wurtzite structure. The SAED results show that three legs of these nanotriplets grow along the [001] direction without apparent defects or phase segregation. Figure S4 (Supporting Information) shows a typical SEM image of these nanotriplets at the initial growth stage. As can be seen, the nanotriplets start to nucleate, and the branches start to sprout from the nucleus at this initial moment. All these results clearly demonstrate that the achieved Sn-doped CdS nanotriplets are high-quality wurtzite structures, with the three legs epitaxially grown on the (001) surfaces of the pregrown nucleus. Moreover, some typical CdS_{1-x}Se_x alloy

nanotriplets with different compositions have also been realized by the same method shown in Figure S5 (Supporting Information), which exhibit nearly the same morphology as the Sn-doped CdS nanotriplets shown in Figure 1. The growth details can be found in the Experimental Section.

To shed light on their optical properties, Figure 2 panels a–d show the top-view optical photographs and dark-field real-color images of a CdS nanotriplet grown on the silicon substrate under a confocal optical system (Figure S6, Supporting Information) with a continuous wavelength (CW) 375 nm laser excitation. The studied nanotriplet has three legs with a length of ~2.5 μm and a diameter of 800 nm. Figure 2e shows a 2D emission mapping of the CdS nanotriplet under a 375 nm CW laser scanning, illustrating a uniform emission image at 509 nm. Positions P₁–P₃ in Figure 2 panels b–d indicate this structure's three typical excitation positions. The PL spectra from the three different positions (Figure 2f–h) exhibit a band-edge emission peak at 509 nm and a broad emission band, which can be attributed to oxygen vacancy induced defect-state emissions.⁴⁶ In addition, the good waveguide effect of the nanotriplet can be observed in the dark-field images (Figure 2b–d), which

indicates that these structures may have a delicate optical confinement cavity. Figure 2i exhibits six real-color images of typical $\text{CdS}_{1-x}\text{Se}_x$ alloy nanotriods with different compositions ($x = 0\text{--}1$) under laser illumination. Spatially resolved μ -PL spectra shown in Figure 2j suggest that these CdSSe alloy nanotriods exhibit continuously tunable spontaneous emissions from 509 nm (CdS) to 712 nm (CdSe) with a full width at half-maximum (fwhm) of around ~ 25 nm. The EDS spectra show that the $\text{CdS}_{1-x}\text{Se}_x$ nanotriods (Figure S7, Supporting Information) contain Cd, Se, and S as their major constituents with varying S and Se ratios and extremely dilute amounts of Sn. From the band-to-band emission peaks in PL spectra and the EDS measured composition, a correlation between the bandgap and composition of $\text{CdS}_{1-x}\text{Se}_x$ nanotriods can be established and shown in Figure 2k. The solid line in Figure 2k shows the best fit of composition-dependent bandgaps of the alloy nanotriods using the virtual crystal approximation with a bowing parameter $b = 0.23$ eV. The composition uniformity was studied by SEM and EDS mapping on two selected $\text{CdS}_{1-x}\text{Se}_x$ alloy nanotriods ($x = 0.17$ and 0.48), and the results are shown in Figures S8 and S9 (Supporting Information), respectively. The EDS elemental maps suggest uniform distributions of the Cd, S, Se, and Sn in these nanotriods. In addition, PL spectra and emission mapping images of these two $\text{CdS}_{1-x}\text{Se}_x$ alloy nanotriods are shown in Figures S10 and S11 (Supporting Information), which indicate the alloy tripods have uniform emissions at 548 and 601 nm with negligible defect-state emissions, respectively.

Results of the structural and optical characterization suggest that these nanotripod structures may simultaneously act as good optical gain and optical confinement cavities for the fabrication of nanoscale lasers.^{47,48} To validate this concept, a 355 nm pulsed laser beam is focused to $\sim 100 \mu\text{m}$ by a microscope to provide optical pumping on these $\text{CdS}_{1-x}\text{Se}_x$ nanotriods. As schematically shown in Figure 3a, the local signal is detected by a spectrometer, and the images are recorded by a CCD camera. Figure 3b shows an optical image of a representative nanotripod, which has three legs with projection lengths of 5.6, 5.6, and 5.7 μm , respectively. Because the angle between the horizontal substrate plane and the legs of the tripod is about 19° (Figure S1, Supporting Information), the projected length is approximately equal to the actual length in this work. Figure 3 panels c–e show a series of PL spectra and corresponding dark-field emission images (inset images) from the three legs of the nanotripod under a 355 nm pulse laser excitation with different pumping powers. It can be seen that the output emission spots ($P_1\text{--}P_3$) from the three legs gradually changed from dark to bright with the increasing power density, which is in agreement with PL spectra in Figure 3c–e, respectively. The PL spectra at spots $P_1\text{--}P_3$ (Figure 3c–e) exhibit a broad and weak spontaneous emission band at ~ 509 nm at a low pumping power density ($18.68 \mu\text{J}/\text{cm}^2$). Sharp emission lines center at 519.23, 520.76, and 518.89 nm start to emerge when the pump power increases beyond the threshold (41.70, 46.56, and $43.89 \mu\text{J}/\text{cm}^2$), respectively, suggesting that stimulated emission occurs in this nanotripod cavity and guides to the tip of the three legs ($P_1\text{--}P_3$). From the experiment results, the threshold of the nanotripod laser is 2 times lower than the thresholds of the conventional CdSSe nanowire lasers ($79.4 \mu\text{J}/\text{cm}^2$)³¹ and much lower than the thresholds of the CdSSe nanoribbon lasers ($68 \text{ MW}/\text{cm}^2$).⁴⁹ Figure 3f shows the intensities of the sharp emission lines as a function of the pumping power density according to the PL spectra of the three spots, which exhibit a superlinear increase

when the power density is above a threshold value, indicating a transition from spontaneous emission to stimulated emission. It is worth noting that the lasing modes (Figure 3g) from the three output spots ($P_1\text{--}P_3$) are slightly different. This is believed to result from the presence of some weak emission lines accompanying each lasing line in almost all the obtained lasing spectra.^{50,51} The narrow line width and the rapid increase of emission intensity collected from three different legs (spots $P_1\text{--}P_3$) demonstrate that stimulated emission can take place in this nanotripod cavity and output from three legs simultaneously.

The mode selection of lasing action can be realized by the coupled cavities by means of Vernier Effect.⁵² Generally, the lasing action is multimode in a single nanowire with only one F–P cavity. As seen, a singly separated leg of Sn-doped CdS nanotripod ($11 \mu\text{m}$ in length) is pumped by a 355 nm pulse laser in Figure S12 (Supporting Information). When the optical pump is above the lasing threshold at $50 \mu\text{J}/\text{cm}^2$, multimode lasing is observed with a measured mode spacing of about 2.1 nm (Figure S12c, Supporting Information). However, the lasing emissions from nanotriods suggest the attractive oscillation cavities in these nanostructures may be able to realize single mode lasing when the cavity size is increased to a certain level. Figure S13 (Supporting Information) presents a theoretical oscillation model, which could act as an equivalent F–P resonator, and the wavelength of stimulated emission can be calculated by the following equation:

$$\lambda = 2nL/k \quad (1)$$

where n is the refractive index of CdS ($n = 2.67$), L ($L = 1/2[(L_1 + L_2) + (L_2 + L_3) + (L_3 + L_1)] = L_1 + L_2 + L_3$) is the total equivalent cavity length of the nanotripod, and k is an integer. The calculated emission wavelength using eq 1 is in good agreement with the actual measured value, as shown in Figure 3h,i. The lasing oscillations are investigated and demonstrated for nanotriods with different dimensions. As shown in Figure 3h, six representative lasing spectra are recorded from triods with different equivalent cavity lengths L from 6.0 to $18.0 \mu\text{m}$ with narrow lasing modes. It can be seen that the lasing peak follows eq 1 and exhibits a continuous red shift with increasing cavity length L . The relationship between laser mode spacing ($\Delta\lambda$) and cavity length (L) are explored by the equation⁵³

$$\Delta\lambda = \lambda^2 / \{2L[n - \lambda(dn/d\lambda)]\} \quad (2)$$

where λ is the lasing wavelength at ~ 520 nm, n is the corresponding refraction index (0.67), L is the equivalent length of nanotripod cavity, and $dn/d\lambda$ is the chromatic dispersion ($-6.89 \mu\text{m}^{-1}$).^{54,55} A nearly linear dependence of the mode spacing ($\Delta\lambda$) on the reciprocal of the cavity length ($1/L$) is observed, as shown in Figure 3i (red pentagram), which is in agreement with the calculations based on the F–P mode spacing relationship using eq 2 (blue sphere). These results further support the high-quality F–P optical cavities formed in nanotriods.

The quality factor (Q) of stimulated emission can be calculated by the following expression

$$Q = \lambda/\delta\lambda \quad (3)$$

where λ is the wavelength of stimulated radiation mode and $\delta\lambda$ is the fwhm of the mode peak. After examining a dozen $\text{CdS}_{1-x}\text{Se}_x$ nanotriods with different compositions, we find that the minimum peak width (fwhm) of the main mode of stimulated radiation is 0.54 nm, as shown in Figure S14 (Supporting Information). Therefore, the Q factor of the nanotripod can be

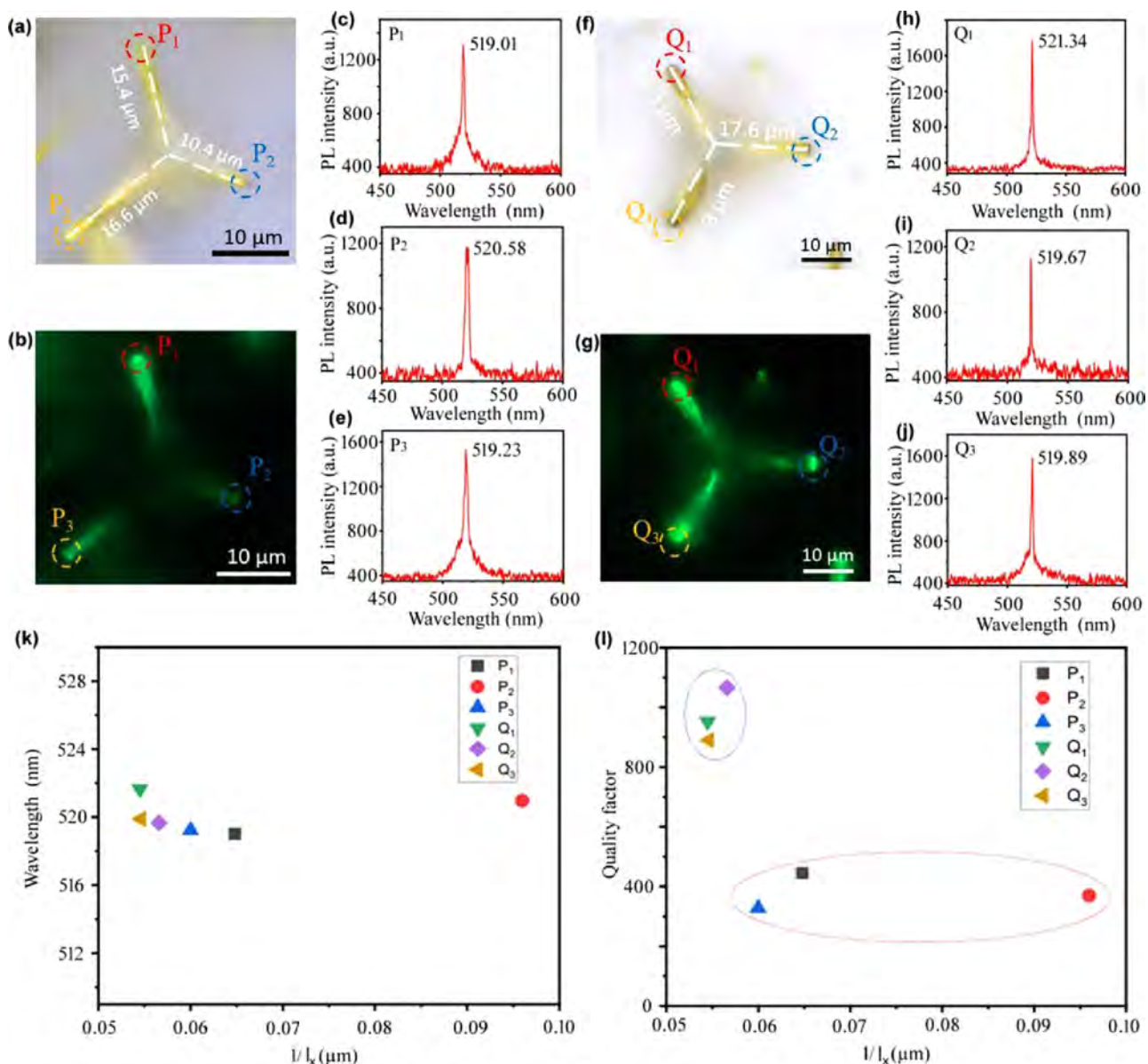


Figure 4. Comparative investigation of stimulated emission from two typical CdS nanotrirod cavities with uniform and nonuniform branches (legs). (a and b) A top-view optical photograph and dark-field image, respectively, of a CdS nanotrirod with nonuniform legs grown on silicon substrate. (c-e) Lasing emission spectra from the tip of the nanotrirod, as shown in (a), pumped with power above the lasing threshold at $100 \mu\text{J}/\text{cm}^2$. (f and g) A top-view optical photograph and dark-field image, respectively, of a CdS nanotrirod with three relatively uniform legs. (h-j) Three lasing emissions from the tip of the tripod, as shown in (f), pumped with power above the lasing threshold at $100 \mu\text{J}/\text{cm}^2$. (k) The lasing emission peak λ plotted as a function of $1/L_x$ ($x = 1, 2, 3$, the length of each leg), and (l) the quality factors Q from different nanotriods (P_1-P_3 and Q_1-Q_3 indicated in the diagram (a) and (f)), respectively.

calculated as 1231. Such a high Q factor demonstrates that nanotriods are high-quality cavities that can be potentially used to fabricate excellent nanoscale lasers.

Moreover, further investigation of the dependence of lasing emission mode on the uniformity of the nanotriod leg length is also investigated. The lasing mode of two different nanotriods, with uniform and nonuniform legs, are studied, and the results are shown in Figure 4. Figure 4 panels a and b give the optical photograph and dark-field emission image of a nonuniform nanotriod with different leg lengths of $L_1 = 15.4 \text{ nm}$, $L_2 = 10.4 \text{ nm}$, $L_3 = 16.6 \text{ nm}$, and an equivalent cavity length $L = L_1 + L_2 + L_3 = 42.4 \mu\text{m}$. Under a 355 nm pulse laser pumping, the three lasing emissions show single modes (Figure 4c–e) at 519.01, 520.58, and 519.23 nm from the three legs of the tripod (P_1-P_3

as indicated in Figure 4a), respectively. In contrast, Figure 4 panels f and g show the optical photograph and dark-field emission image of a nanotriod with three nearly uniform legs ($L = L_1 + L_2 + L_3 = 18.3 + 17.6 + 18.3 = 54.2 \mu\text{m}$). Lasing emission peaks (Figure 4h–j) with single modes at 521.34, 519.67, and 519.89 nm are also observed from the three legs (Q_1-Q_3 as indicated in Figure 4f), respectively, from this nanotriod with uniform leg lengths. As presented in Figure 4k, the lasing mode wavelengths from the different legs for both uniform and nonuniform nanotriods are very similar for the same cavity. This suggests that a single-mode stimulated emission takes place from a single-nanotriod cavity, showing almost no correlation with the length of legs. However, each leg's lasing emission Q factor (Figure 4l) is nearly the same in the

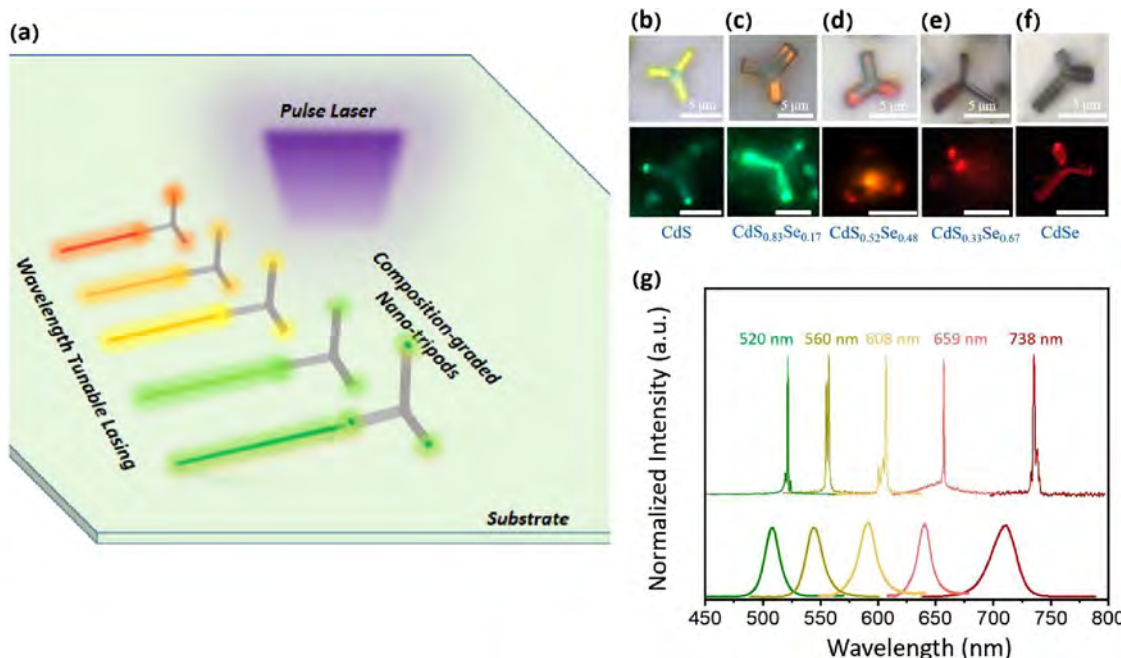


Figure 5. Wavelength-tunable lasing of $\text{CdS}_{1-x}\text{Se}_x$ alloy nanotripods. (a) A schematic diagram of the lasing measurements on $\text{CdS}_{1-x}\text{Se}_x$ alloy nanotripods with different compositions. (b–f) Optical photographs and dark-field real-color images of some typical $\text{CdS}_{1-x}\text{Se}_x$ alloy nanotripods under an unfocused 355 nm pulsed laser illumination. All the scale bars are 5 μm . (g) Corresponding PL spectra of these nanotripods below and above the lasing threshold.

same nanotriod, whereas Q factors for the uniform nanotriod are >2 times higher than those from the nonuniform one. Moreover, these nanotripods have the potential to serve in integrated nanophotonic devices; a single CdSSe nanotriod and a waveguide (CsPbCl_3 nanowire) are coupled together on a chip, as shown in Figures S15 and S16 (Supporting Information). The micromanipulation is carried out by a homemade fiber probe mounted on a precisely controlled 3-dimensional moving stage.

Finally, lasing from nanotripods with wavelength-tunable emission ranging from 520 to 738 nm is realized by adjusting the composition of the $\text{CdS}_{1-x}\text{Se}_x$. A schematic diagram of the CVD growth of these $\text{CdS}_{1-x}\text{Se}_x$ nanotripods and the corresponding growth parameters are shown in Figure S5 (Supporting Information). Figure 5a depicts a schematic diagram of the experimental configuration for the optically pumped PL measurements. A pulse laser beam (355 nm) was focused (spot size, $\sim 100 \mu\text{m}$) by an objective lens and then locally pumped on these nanotripods. The local optical signals were then detected by a spectrometer, and the far-field optical images were recorded by a charge coupled device (CCD) color camera. Figure 5 panels b–f show five representative optical photographs and dark-field real-color emission images of $\text{CdS}_{1-x}\text{Se}_x$ alloy nanotripods with different compositions ($x = 0, 0.17, 0.48, 0.67, 1$), demonstrating various emission colors from green to orange to red. Corresponding EDS spectra of these alloy nanotripods are shown in Figure S17 (Supporting Information). PL spectra of these nanotripods shown in Figure 5g show that the lasing emission wavelength can be continuously tuned from 520 to 738 nm, providing an excellent platform for the fabrication of broad-wavelength-tunable nanotripods lasers. Notably, all the sharp stimulated emission lines appear at longer wavelengths (lower energies) compared with results for their corresponding spontaneous emission peaks. This can be attributed to the self-absorption process during the light

transmission and oscillation. To the best of our knowledge, this is a vitally important report of broadly tunable color nanolasers based on the nanotripods cavities.

CONCLUSION

In conclusion, high-quality $\text{CdS}_{1-x}\text{Se}_x$ nanotriod structures with compositions from $x = 0$ to 1 were synthesized using the CVD strategy. Microstructure characterization reveals that these nanotripods have a single-crystalline structure with tunable compositions. Photoluminescence observations indicate that these tripods have good waveguide effects through the three branches (legs). Moreover, under a pulse laser illumination, the nanotripods exhibit PL emissions from broad spontaneous emissions to strongly stimulated emissions when the optical pumping power increases to above a threshold value. Additionally, these $\text{CdS}_{1-x}\text{Se}_x$ nanotripods can be used as high-quality equivalent F-P cavities for single-mode tunable nanolasers with emissions from 520 to 738 nm at room temperature. The development of a nanoscale laser source with tunable wavelengths provides an attractive design for realizing single-mode lasers and exciting opportunities for diverse applications in integrated photonics.

EXPERIMENTAL SECTION

Material Preparation and Characterizations. $\text{CdS}_{1-x}\text{Se}_x$ nanotripods were grown via a conventional CVD strategy, as schematically shown in Figure S5 (Supporting Information). Sources and reagents were purchased from Alfa Aesar. A horizontal furnace (OTF-1200X) with a 2 in. quartz tube (inner diameter 45 mm, length 180 cm) was used. For example, before the growth of tin-doped CdS nanotripods, two alumina boats (74 mm in length) filled with CdS powder (Alfa Aesar, 99.99%, 0.07 g) and Sn powder (Alfa Aesar, 99.99%, 0.035 g) were placed in the center and upstream of the heating zone, respectively. Several pieces of Si (4 mm \times 10 mm) were placed at the deposition area. Before heating, N_2 gas was introduced into the system at a flow rate of 60 sccm for 30 min to purge the air and moisture from

the tube. After that, the N₂ flow was increased to 120 sccm, while the pressure in the tube was maintained at 220 Torr. Then the furnace was heated to 780 °C at a rate of 26 °C min⁻¹ and the growth time was 90 min. After the growth, the furnace was naturally cooled to room temperature. Similar growth processes were used to grow alloys with different compositions with slightly different growth parameters, as shown in Figure S5 (Supporting Information).

Characterization. The morphology and chemical composition of these nanostructures were investigated via scanning electron microscopy (SEM, Hitachi, S-4800, Japan) with energy dispersive X-ray spectroscopy (EDS) capability at an accelerating voltage of 5.0 kV. The microstructures and crystal structures were determined by transmission electron microscopy (TEM, JEM-F200). The optical images, PL spectra, and mapping were completed by a home-built confocal optical system. A laser beam (375 nm) was focused to a spot size of ~0.8 μm by a microscope lens (Nikon, ×100) and locally excited the nanostructures. The PL spectra were recorded by an Ocean Optics Spectrometer (Maya Pro2000), and real color images were recorded by a CCD camera. Stimulated emission properties were studied using a 355 nm pulse laser illumination, which was focused to 100 μm. A nanotriod was selected and transferred to an MgF₂ substrate by a 3D manipulator with homemade fiber probes for characterization. Because of the challenges in monolithically integrated on-chip light sources, a micromanipulation method by a fiber probe is proposed to fabricate on-chip tunable lasers in this work. The micromanipulation process is shown in Figure S18 (Supporting Information). Figure S19 (Supporting Information) exhibits the optical photograph and corresponding real-color image of the constructed on-chip composition-tunable nanotriods, which could be used to realize on-chip wavelength continuously tunable lasing. Dark-field PL emission images and spectra were collected by a CCD camera and optical spectrometer (Maya Pro2000).

ASSOCIATED CONTENT

SI Supporting Information

The Supporting Information is available free of charge at <https://pubs.acs.org/doi/10.1021/acsnano.2c04632>.

SEM image of Sn-doped CdS nanotriods recorded at an angle of 45°; in situ EDS spectrum of a CdS nanotriod; optical microscope images; typical SEM image of CdS nanotriods at the initial stage of the growth; experimental setup and growth parameters; diagram of the confocal microscope system; EDS spectra from some selected CdS_{1-x}Se_x alloy nanotriods; SEM images; optical characterization and structural investigation of some Sn-doped alloyed CdS_{1-x}Se_x nanotriods; optical characterization of a singly separated leg of Sn-doped CdS nanotriod; theoretical oscillation model in the nanotriod structure; dark-field emission image and the corresponding lasing emission spectrum of a typical CdS_{0.33}Se_{0.67} alloy nanotriod; optical photograph of a single CdS_{0.71}Se_{0.29} nanotriod coupled with a single CsPbCl₃ nanowire; transfer process of the nanotriod by a homemade fiber probe; optical microscope images of the micromanipulation process by a homemade fiber probe ([PDF](#))

AUTHOR INFORMATION

Corresponding Authors

Pengfei Guo — College of Physics and Optoelectronics, Key Laboratory of Advanced Transducers and Intelligent Control System Ministry of Education, Taiyuan University of Technology, Taiyuan 030024, China; Department of Physics, City University of Hong Kong, Kowloon, Hong Kong 999077, China; [orcid.org/0000-0002-4785-0753](#); Email: guopengfei@tyut.edu.cn

China; [orcid.org/0000-0002-4785-0753](#);

Email: guopengfei@tyut.edu.cn

Liantuan Xiao — College of Physics and Optoelectronics, Key Laboratory of Advanced Transducers and Intelligent Control System Ministry of Education, Taiyuan University of Technology, Taiyuan 030024, China; [orcid.org/0000-0003-2690-6460](#); Email: xlt@sxu.edu.cn

Johnny C. Ho — Department of Materials Science and Engineering, City University of Hong Kong, Kowloon, Hong Kong 999077, China; Institute for Materials Chemistry and Engineering, Kyushu University, Fukuoka 816-8580, Japan; [orcid.org/0000-0003-3000-8794](#); Email: johnnyho@cityu.edu.hk

Kin Man Yu — Department of Physics, City University of Hong Kong, Kowloon, Hong Kong 999077, China; Email: kinmanyu@cityu.edu.hk

Authors

Qian Yang — College of Physics and Optoelectronics, Key Laboratory of Advanced Transducers and Intelligent Control System Ministry of Education, Taiyuan University of Technology, Taiyuan 030024, China

Xia Shen — College of Physics and Optoelectronics, Key Laboratory of Advanced Transducers and Intelligent Control System Ministry of Education, Taiyuan University of Technology, Taiyuan 030024, China

Qihang Lv — College of Physics and Optoelectronics, Key Laboratory of Advanced Transducers and Intelligent Control System Ministry of Education, Taiyuan University of Technology, Taiyuan 030024, China

Yuying Hao — College of Physics and Optoelectronics, Key Laboratory of Advanced Transducers and Intelligent Control System Ministry of Education, Taiyuan University of Technology, Taiyuan 030024, China; [orcid.org/0000-0002-9691-7109](#)

Complete contact information is available at: <https://pubs.acs.org/10.1021/acsnano.2c04632>

Author Contributions

#P.G., Q.Y., and X.S. contributed equally to this work.

Notes

The authors declare no competing financial interest.

ACKNOWLEDGMENTS

The authors are grateful to the start-up funding from Taiyuan University of Technology and Shanxi Basic Research Program Project (No. 20210302123128) for financial support. K.M.Y. acknowledges support of the CityU SGP (Grant No. 9380076). J.C.H. acknowledges support from General Research Fund (CityU 11306520) of the Research Grants Council of Hong Kong SAR, China.

REFERENCES

- (1) Ning, C. Z.; Dou, L.; Yang, P. Bandgap Engineering in Semiconductor Alloy Nanomaterials with Widely Tunable Compositions. *Nat. Rev. Mater.* **2017**, *2*, 17070.
- (2) Quan, L. N.; Kang, J.; Ning, C. Z.; Yang, P. Nanowires for Photonics. *Chem. Rev.* **2019**, *119*, 9153–9169.
- (3) Pan, A.; Liu, R.; Sun, M.; Ning, C. Z. Spatial Composition Grading of Quaternary ZnCdSSe Alloy Nanowires with Tunable Light Emission between 350 and 710 nm on a Single Substrate. *ACS Nano* **2010**, *4*, 671–680.

- (4) Guo, P.; Zhuang, X.; Xu, J.; Zhang, Q.; Hu, W.; Zhu, X.; Wang, X.; Wan, Q.; He, P.; Zhou, H.; Pan, A. Low-Threshold Nanowire Laser Based on Composition-Symmetric Semiconductor Nanowires. *Nano Lett.* **2013**, *13*, 1251–1256.
- (5) Dou, L.; Lai, M.; Kley Christopher, S.; Yang, Y.; Bischak Connor, G.; Zhang, D.; Eaton Samuel, W.; Ginsberg Naomi, S.; Yang, P. Spatially Resolved Multicolor CsPbX_3 Nanowire Heterojunctions via Anion Exchange. *Proc. Natl. Acad. Sci. U.S.A.* **2017**, *114*, 7216–7221.
- (6) Fan, F.; Turkdogan, S.; Liu, Z.; Shelhammer, D.; Ning, C. Z. A Monolithic White Laser. *Nat. Nanotechnol.* **2015**, *10*, 796–803.
- (7) Pan, A.; Liu, R.; Sun, M.; Ning, C. Z. Quaternary Alloy Semiconductor Nanobelts with Bandgap Spanning the Entire Visible Spectrum. *J. Am. Chem. Soc.* **2009**, *131*, 9502–9503.
- (8) Yang, Z.; Wang, D.; Meng, C.; Wu, Z.; Wang, Y.; Ma, Y.; Dai, L.; Liu, X.; Hasan, T.; Liu, X.; Yang, Q. Broadly Defining Lasing Wavelengths in Single Bandgap-Graded Semiconductor Nanowires. *Nano Lett.* **2014**, *14*, 3153–3159.
- (9) Fu, Y.; Zhu, H.; Stoumpos, C. C.; Ding, Q.; Wang, J.; Kanatzidis, M. G.; Zhu, X.; Jin, S. Broad Wavelength Tunable Robust Lasing from Single-Crystal Nanowires of Cesium Lead Halide Perovskites (CsPbX_3 , X = Cl, Br, I). *ACS Nano* **2016**, *10*, 7963–7972.
- (10) Zhu, H.; Fu, Y.; Meng, F.; Wu, X.; Gong, Z.; Ding, Q.; Gustafsson, M. V.; Trinh, M. T.; Jin, S.; Zhu, X. Y. Lead Halide Perovskite Nanowire Lasers with Low Lasing Thresholds and High Quality Factors. *Nat. Mater.* **2015**, *14*, 636–642.
- (11) Dai, J.; Zhou, P.; Lu, J.; Zheng, H.; Guo, J.; Wang, F.; Gu, N.; Xu, C. The Excitonic Photoluminescence Mechanism and Lasing Action in Band-gap-tunable $\text{CdS}_{1-x}\text{Se}_x$ Nanostructures. *Nanoscale* **2016**, *8*, 804–811.
- (12) Ma, Y.; Guo, X.; Wu, X.; Dai, L.; Tong, L. Semiconductor Nanowire Lasers. *Adv. Opt. Photonics* **2013**, *5*, 216–273.
- (13) Duan, X.; Huang, Y.; Agarwal, R.; Lieber, C. M. Single-Nanowire Electrically Driven Lasers. *Nature* **2003**, *421*, 241–245.
- (14) Chu, S.; Wang, G.; Zhou, W.; Lin, Y.; Chernyak, L.; Zhao, J.; Kong, J.; Li, L.; Ren, J.; Liu, J. Electrically Pumped Waveguide Lasing from ZnO Nanowires. *Nat. Nanotechnol.* **2011**, *6*, 506–510.
- (15) Vugt, L. K.; Piccione, B.; Cho, C.-H.; Aspetti, C.; Wirshba, A. D.; Agarwal, R. Variable Temperature Spectroscopy of As-Grown and Passivated CdS Nanowire Optical Waveguide Cavities. *J. Phys. Chem. A* **2011**, *115*, 3827–3833.
- (16) van Vugt, L. K.; Piccione, B.; Agarwal, R. Incorporating Polaritonic Effects in Semiconductor Nanowire Waveguide Dispersion. *Appl. Phys. Lett.* **2010**, *97*, 061115.
- (17) Huang, M. H.; Mao, S.; Feick, H.; Yan, H.; Wu, Y.; Kind, H.; Weber, E.; Russo, R.; Yang, P. Room-Temperature Ultraviolet Nanowire Nanolasers. *Science* **2001**, *292*, 1897–1899.
- (18) Eaton, S. W.; Fu, A.; Wong, A. B.; Ning, C. Z.; Yang, P. Semiconductor Nanowire Lasers. *Nat. Rev. Mater.* **2016**, *1*, 16028.
- (19) Gao, H.; Fu, A.; Andrews, S. C.; Yang, P. Cleaved-Coupled Nanowire Lasers. *Proc. Natl. Acad. Sci. U.S.A.* **2013**, *110*, 865–869.
- (20) Huang, M. H.; Mao, S.; Feick, H.; Yan, H.; Wu, Y.; Kind, H.; Weber, E.; Russo, R.; Yang, P. Room-Temperature Ultraviolet Nanowire Nanolasers. *Science* **2001**, *292*, 1897–1899.
- (21) Zhang, S.; Zhukovskyi, M.; Jankó, B.; Kuno, M. Progress in Laser Cooling Semiconductor Nanocrystals and Nanostructures. *Npg Asia Mater.* **2019**, *11*, 54.
- (22) Wang, Y.; Guan, X.; Li, D.; Cheng, H. C.; Duan, X.; Lin, Z.; Duan, X. Chemical Vapor Deposition Growth of Single-Crystalline Cesium Lead Halide Microplatelets and Heterostructures for Optoelectronic Applications. *Nano Res.* **2017**, *10*, 1223–1233.
- (23) Grivas, C.; Li, C.; Andreakou, P.; Wang, P.; Ding, M.; Brambilla, G.; Manna, L.; Lagoudakis, P. Single-Mode Tunable Laser Emission in the Single-Exciton Regime from Colloidal Nanocrystals. *Nat. Commun.* **2013**, *4*, 2376.
- (24) Liu, P.; He, X.; Ren, J.; Liao, Q.; Yao, J.; Fu, H. Organic-Inorganic Hybrid Perovskite Nanowire Laser Arrays. *ACS Nano* **2017**, *11*, 5766–5773.
- (25) Xing, G.; Mathews, N.; Lim, S. S.; Yantara, N.; Liu, X.; Sabba, D.; Grätzel, M.; Mhaisalkar, S.; Sum, T. C. Low-Temperature Solution-Processed Wavelength-Tunable Perovskites for Lasing. *Nat. Mater.* **2014**, *13*, 476–480.
- (26) Xu, J.; Ma, L.; Guo, P.; Zhuang, X.; Zhu, X.; Hu, W.; Duan, X.; Pan, A. Room-Temperature Dual-Wavelength Lasing from Single-Nanoribbon Lateral Heterostructures. *J. Am. Chem. Soc.* **2012**, *134*, 12394–12397.
- (27) Zhuang, X.; Guo, P.; Zhang, Q.; Liu, H.; Li, D.; Hu, W.; Zhu, X.; Zhou, H.; Pan, A. Lateral Composition-Graded Semiconductor Nanoribbons for Multi-Color Nanolasers. *Nano Res.* **2016**, *9*, 933–941.
- (28) Zhang, Q.; Liu, H.; Guo, P.; Li, D.; Fan, P.; Zheng, W.; Zhu, X.; Jiang, Y.; Zhou, H.; Hu, W.; Zhuang, X.; Liu, H.; Duan, X.; Pan, A. Vapor Growth and Interfacial Carrier Dynamics of High-Quality $\text{CdS}-\text{CdSSe}-\text{CdS}$ Axial Nanowire Heterostructures. *Nano Energy* **2017**, *32*, 28–35.
- (29) Guo, P.; Liu, D.; Shen, X.; Lv, Q.; Wu, Y.; Yang, Q.; Li, P.; Hao, Y.; Ho, J. C.; Yu, K. M. On-wire Axial Perovskite Heterostructures for Monolithic Dual-wavelength Laser. *Nano Energy* **2022**, *92*, 106778.
- (30) Ha, S.-T.; Su, R.; Xing, J.; Zhang, Q.; Xiong, Q. Metal Halide Perovskite Nanomaterials: Synthesis and Applications. *Chem. Sci.* **2017**, *8*, 2522–2536.
- (31) Feng, J.; Yan, X.; Zhang, Y.; Wang, X.; Wu, Y.; Su, B.; Fu, H.; Jiang, L. Liquid Knife” to Fabricate Patterning Single-Crystalline Perovskite Microplates toward High-Performance Laser Arrays. *Adv. Mater.* **2016**, *28*, 3732–3741.
- (32) Lethy, K. J.; Beena, D.; Vinod Kumar, R.; Mahadevan Pillai, V. P.; Ganeshan, V.; Sathe, V. Structural, Optical and Morphological Studies on Laser Ablated Nanostructured WO_3 Thin Films. *Appl. Surf. Sci.* **2008**, *254*, 2369–2376.
- (33) Yasumaru, N.; Miyazaki, K.; Kiuchi, J. Femtosecond-Laser-Induced Nanostructure Formed on Hard Thin Films of TiN and DLC. *Appl. Phys. A: Mater. Sci. Process.* **2003**, *76*, 983–985.
- (34) Zhang, Q.; Su, R.; Liu, X.; Xing, J.; Sum, T. C.; Xiong, Q. High-Quality Whispering-Gallery-Mode Lasing from Cesium Lead Halide Perovskite Nanoplatelets. *Adv. Funct. Mater.* **2016**, *26*, 6238–6245.
- (35) Xiao, Y.; Meng, C.; Wang, P.; Ye, Y.; Yu, H.; Wang, S.; Gu, F.; Dai, L.; Tong, L. Single-Nanowire Single-Mode Laser. *Nano Lett.* **2011**, *11*, 1122–1126.
- (36) Zhang, Q.; Shang, Q.; Su, R.; Do, T. T. H.; Xiong, Q. Halide Perovskite Semiconductor Lasers: Materials, Cavity Design, and Low Threshold. *Nano Lett.* **2021**, *21*, 1903–1914.
- (37) Pan, A.; Zhou, W.; Leong, E. S. P.; Liu, R.; Chin, A. H.; Zou, B.; Ning, C. Z. Continuous Alloy-Composition Spatial Grading and Superbroad Wavelength-Tunable Nanowire Lasers on a Single Chip. *Nano Lett.* **2009**, *9*, 784–788.
- (38) Liu, Y. K.; Zaprien, J. A.; Shan, Y. Y.; Tang, H.; Lee, C. S.; Lee, S. T. Wavelength-Tunable Lasing in Single-Crystal $\text{CdS}_{1-x}\text{Se}_x$ Nanoribbons. *Nanotechnology* **2007**, *18*, 365606.
- (39) Liu, Y.; Zaprien, J. A.; Shan, Y. Y.; Geng, C. Y.; Lee, C. S.; Lee, S. T. Wavelength-Controlled Lasing in $\text{Zn}_x\text{Cd}_{1-x}\text{S}$ Single-Crystal Nanoribbons. *Adv. Mater.* **2005**, *17*, 1372–1377.
- (40) Ma, R.-M.; Yin, X.; Oulton, R. F.; Sorger, V. J.; Zhang, X. Multiplexed and Electrically Modulated Plasmon Laser Circuit. *Nano Lett.* **2012**, *12*, 5396–5402.
- (41) Li, J.; Meng, C.; Liu, Y.; Wu, X.; Lu, Y.; Ye, Y.; Dai, L.; Tong, L.; Liu, X.; Yang, Q. Wavelength Tunable CdSe Nanowire Lasers Based on the Absorption-Emission-Absorption Process. *Adv. Mater.* **2013**, *25*, 833–837.
- (42) Lu, Y.-J.; Wang, C.-Y.; Kim, J.; Chen, H.-Y.; Lu, M.-Y.; Chen, Y.-C.; Chang, W.-H.; Chen, L.-J.; Stockman, M. I.; Shih, C.-K.; Gwo, S. All-Color Plasmonic Nanolasers with Ultralow Thresholds: Autotuning Mechanism for Single-Mode Lasing. *Nano Lett.* **2014**, *14*, 4381–4388.
- (43) Liu, X.; Zhang, Q.; Xiong, Q.; Sum, T. C. Tailoring the Lasing Modes in Semiconductor Nanowire Cavities Using Intrinsic Self-Absorption. *Nano Lett.* **2013**, *13*, 1080–1085.
- (44) Fu, Y.; Wu, T.; Wang, J.; Zhai, J.; Shearer, M. J.; Zhao, Y.; Hamers, R. J.; Kan, E.; Deng, K.; Zhu, X. Y.; Jin, S. Stabilization of the Metastable Lead Iodide Perovskite Phase via Surface Functionalization. *Nano Lett.* **2017**, *17*, 4405–4414.

- (45) Zhang, Q.; Ha, S. T.; Liu, X.; Sum, T. C.; Xiong, Q. Room-Temperature Near-Infrared High-Q Perovskite Whispering-Gallery Planar Nanolasers. *Nano Lett.* **2014**, *14*, 5995–6001.
- (46) Lu, Y.; Gu, F.; Meng, C.; Yu, H.; Ma, Y.; Fang, W.; Tong, L. M. Multicolour Laser from A Single Bandgap-Graded CdSSe Alloy Nanoribbon. *OPTICS EXPRESS* **2013**, *21*, 22314.
- (47) Xu, J.; Zhuang, X.; Guo, P.; Zhang, Q.; Ma, L.; Wang, X.; Zhu, X.; Pan, A. Dilute Tin-Doped CdS Nanowires for Low-Loss Optical Waveguiding. *J. Mater. Chem.C* **2013**, *1*, 4391–4396.
- (48) Sirbuly, D. J.; Law, M.; Pauzauskis, P.; Yan, H.; Maslov, A. V.; Knutsen, K.; Ning, C.-Z.; Saykally, R. J.; Yang, P. Optical Routing and Sensing with Nanowire Assemblies. *P. Natl. Acad. Sci. USA* **2005**, *102*, 7800–7805.
- (49) Friedman, R. S.; McAlpine, M. C.; Ricketts, D. S.; Ham, D.; Lieber, C. M. High-Speed Integrated Nanowire Circuits. *Nature* **2005**, *434*, 1085–1085.
- (50) Johnson, J. C.; Choi, H.-J.; Knutsen, K. P.; Schaller, R. D.; Yang, P.; Saykally, R. J. Single Gallium Nitride Nanowire Lasers. *Nat. Mater.* **2002**, *1*, 106–110.
- (51) He, L.; Özdemir, S. K.; Yang, L. Whispering Gallery Microcavity Lasers. *Laser Photonics Rev.* **2013**, *7*, 60–82.
- (52) Xu, E.; Zhang, X.; Zhou, L.; Zhang, Y.; Yu, Y.; Li, X.; Huang, D. Ultrahigh-Q Microwave Photonic Filter with Vernier Effect and Wavelength Conversion in A Cascaded Pair of Active Loops. *Opt. Lett.* **2010**, *35*, 1242–1244.
- (53) Zhang, Q.; Zhu, X.; Li, Y.; Liang, J.; Chen, T.; Fan, P.; Zhou, H.; Hu, W.; Zhuang, X.; Pan, A. Nanolaser Arrays Based on Individual Waved CdS Nanoribbons. *Laser Photonics Rev.* **2016**, *10*, 458–464.
- (54) Bieniewski, T. M.; Czyzak, S. J. Refractive Indexes of Single Hexagonal ZnS and CdS Crystals. *J. Opt. Soc. Am.* **1963**, *53*, 496–497.
- (55) Gomez, M. S.; Guerra, J. M.; Vilches, F. Weighted Nonlinear Regression Analysis of A Sellmeier Expansion: Comparison of Several Nonlinear Fits of CdS Dispersion. *Appl. Opt.* **1985**, *24*, 1147–1150.

□ Recommended by ACS

Ultrahigh Green and Red Optical Gain Cross Sections from Solutions of Colloidal Quantum Well Heterostructures

Savas Delikanli, Hilmi Volkan Demir, et al.

FEBRUARY 25, 2021

THE JOURNAL OF PHYSICAL CHEMISTRY LETTERS

READ ▶

Highly Luminescent Gradient Alloy CdSe_{1-x}S_x Nanoplatelets with Reduced Reabsorption for White-Light Generation

Bedil M. Saidzhonov, Roman B. Vasiliev, et al.

OCTOBER 14, 2020

ACS PHOTONICS

READ ▶

Enhanced Emission from Bright Excitons in Asymmetrically Strained Colloidal CdSe/Cd_xZn_{1-x}Se Quantum Dots

Igor Fedin, Scott A. Crooker, et al.

SEPTEMBER 02, 2021

ACS NANO

READ ▶

Self-Assembled PbS/CdS Quantum Dot Films with Switchable Symmetry and Emission

Dorota Grzelak, Wiktor Lewandowski, et al.

SEPTEMBER 04, 2019

CHEMISTRY OF MATERIALS

READ ▶

Get More Suggestions >